Combining Surface-Induced Dissociation and Charge Detection Mass Spectrometry to Reveal the Native Topology of Heterogeneous Protein Complexes

Chen Du[1,2]; Sean P. Cleary[2]; Marius M. Kostelic[1,2]; Benjamin J. Jones[1,2]; Jared O. Kafader[3]; Vicki H. Wysocki[1,2,*]

[1]Department of Chemistry and Biochemistry, The Ohio State University, Columbus, OH, USA;

[2]Resource for Native MS Guided Structural Biology, The Ohio State University, Columbus, OH, USA;

[3]Departments of Chemistry, Molecular Biosciences, The Chemistry of Life Processes Institute, The Proteomics Center of Excellence at Northwestern University, Evanston, IL, USA

*Corresponding author: wysocki.11@osu.edu

Author Contributions: CD collected and analyzed the CDMS-SID experiments. SC and BJ desgined and wrote the Python-based data processing algorithm. MK initiated the SID analysis of AAV and helped with the UniDec data processing. JOK assisted in the optimization of the CDMS tuning and raw data processing.VHW conceived and directed the project. The manuscript was written through contributions of all authors. All authors have given approval of the final version of the manuscript.

Abstract

Charge detection mass spectrometry (CDMS) enables the direct mass measurement of heterogenous samples on the megadalton scale, as the charge state for a single ion is determined simultaneously with mass to charge ratio (*m/z*). Surface-induced dissociation (SID) is an effective activation method to dissociate the noncovalent protein complexes without extensive gas-phase restructuring, producing various subcomplexes reflective of the native protein topology. Here, we demonstrate that using CDMS after SID on the Orbitrap platform offers subunit connectivity, topology, proteoform information, and relative interfacial strengths of the intact macromolecular assemblies. SID dissects the capsids (~3.7 MDa) of adeno-associated viruses (AAVs) into trimer-containing fragments (3mer, 6mer, 9mer, 15mer, etc) that can be detected by the individual ion mass spectrometry (I2MS) approach on Orbitrap instruments. SID coupled to CDMS provides unique structural insights into heterogenous assembles that are not obtained by traditional MS measurements.

Introduction

Native mass spectrometry (nMS) has emerged as a powerful tool for structural biology that has advantages in sensitivity, speed, and tolerance of sample heterogeneity and is complementary to classical techniques,[1-4] such as nuclear magnetic resonance, X-ray crystallography, and cryo-electron microscopy. The ability of nMS to preserve non-covalent interactions in the gas phases allows the determination of the native structure and stoichiometry of large protein complexes.[5, 6] To determine this stoichiometric information of a given analyte, the charge state distribution in the mass-to-charge (*m/z*) spectrum must be resolved to determine the mass.[7] However, resolving the charge state distribution can be challenging for heterogeneous macromolecular assemblies. The heterogeneity arising from sequence variants, post-translational modifications, proteoforms, counterions, and residual salts/solvents, causes peak broadening and sometimes makes it impossible to resolve charge states.[8] Single-particle charge-detection mass spectrometry (CDMS) can circumvent this limitation by determining the charge and *m/z* of individual ions simultaneously.[9, 10] Previously, CDMS has been conducted on mainly house-built ion traps,[11-15] and recent work has emerged on commercial Orbitrap platforms.[16-19] The ability to directly detect charges extends the application of nMS to highly heterogenous complexes in the megadalton range, including ribosomes,[20] vaccines,[21] and intact virus particles.[22, 23] Due to the growing applications in gene therapy, CDMS is used in the characterization of adeno-associated viruses (AAVs), including capsid assembly,[24] thermal stability,[25, 26] genome truncations[27], and product heterogeneity.[28, 29]

Gas phase dissociation is commonly employed in nMS to gain structural information including subunit connectivity, ligand binding sites, and topology of macromolecular complexes.[30-33] Collision-induced dissociation (CID), one of the most common activation methods, produces unfolded, highly charged monomers and the complementary (N-1)-mers through multiple-step and low-energy collisions with background gas molecules.[34, 35] CID allows slow accumulation of internal energy and results in restructuring of isolated analyte ions.[36] Although it provides useful stoichiometry information, limited direct information on subunit connectivity is revealed. To probe the quaternary structure of protein complexes, surface-induced dissociation (SID) has emerged as an alternative dissociation method. Unlike CID, SID involves a fast, high-energy deposition process and assists analytes to overcome high-energy barriers.[37, 38] In SID, analyte ions are typically accelerated and directed to collide with a gold surface coated with a monolayer of fluorocarbon chains.[39, 40] Stainless steel, coated with background contaminants, is also used as the collision surface in the recent development of the SID device.[41] SID enables the dissociation of a complex without extensive restructuring and the resulting subcomplexes are more reflective of the solution phase structure.[42-45] At low collision energies, SID tends to break the weakest non-covalent interfaces, making it a powerful tool to determine relative interfacial strengths and reflect the subunit connectivity of the protein complexes.[46]

As part of nMS, SID is also hampered by sample heterogeneity. The SID-produced fragments of a heterogeneous sample are structurally informative but can be difficult to distinguish from each other or precursor ions if they have overlapping charge states. To overcome these issues, CDMS offers an alternative way to separate overlapping species, even for instruments where ion mobility is not commercially available, or isotopes are not resolved. Here, we take advantages of both technologies (SID and CDMS) and integrate them into one workflow to determine detailed structural information for intact macromolecular assemblies. The CDMS approach used here has been developed and described by Kelleher and colleagues as individual ion mass spectrometry (I2MS) and selective temporal overview of resonant ions (STORI) process.[18, 47] This approach has been recently commercialized as Direct Mass Technology Mode. We first performed SID-CDMS on both homomeric and heteromeric complexes, GroEL and human 20S proteasome,

respectively. We then applied this approach to the megadalton range and characterized the quaternary structure of an empty adeno associated viral (AAV) capsid, which are currently being used as gene therapy delivery systems.[48-50] A house-built algorithm was employed to plot the resulting *m/z* values in 2D against the resulting charge and mass of all the data collected during the SID-CDMS experiment. SID-CDMS spectra were further processed and deconvolved using UniDec Charge Detection (UniDecCD).[51]

Experimental Section

Samples

GroEL was purchased from Millipore Sigma (St. Louis, MO, USA) and refolded with the presence of ATP using a published protocol.[52] Human 20S proteasome was purchased from Enzo Biochem (New York, NY, USA). Empty AAV8 was purchased from Virovek (Hayward, CA, USA). GroEL and AAV samples were buffer exchanged by resuspending the particles in 200 mM ammonium acetate and concentrating/diluting with 30 or 100 kDa molecular weight Amicon Ultra centrifugal filters (Merck Millipore, Burlington, MA, USA), at least three consecutive times. Proteosome was buffer-exchanged into 150 mM ammonium acetate using Micro Bio-Spin P6 spin columns with a 6 kDa cutoff (Bio-Rad, Hercules, CA, USA).

Streptavidin (SA) was purchased from Thermo Scientific Pierce (Rockford, IL, USA). C reactive protein human recombinant (CRP), pyruvate kinase (PK) from rabbit muscle, and glutamate dehydrogenase (GDH) from bovine liver were purchased from Millipore Sigma (St. Louis, MO, USA). SA, CRP, PK, and GDH were buffer-exchanged into 200 mM ammonium acetate using Micro Bio-Spin P6 spin columns with a 6 kDa cutoff (Bio-Rad, Hercules, CA, USA). SA, CRP, PK, GDH, and GroEL were used to construct the charge calibration function.

Mass spectrometry

All experiments were performed on a Q Exactive Ultra High Mass Range (UHMR) Orbitrap MS (Thermo Fisher Scientific, Bremen, Germany), which has been modified to include SID.[39] All single-particle charge-detection data were acquired using the Selective Temporal Overview of Resonant Ions (STORI) analysis by Kafader et. al.[18, 47] An aliquot of 1–2 µL sample was loaded into borosilicate capillaries (prepared in-house) for nano-ESI. Instrument parameters were optimized for the transmission of high-mass ions. Therefore, ion transfer target *m/z* and detector optimization were set to high *m/z*. In-source trapping was enabled with a desolvation voltage ranging between -5 V and -100 V. The ion transfer optics (injection flatapole, inter-flatapole, and bent flatapole lens) were set to 5, 3, and 2 V for GroEL and proteosome and 10, 10, and 9 V for AAV8. N2 was used as collision gas for all experiments in the range of 2×10^{-10} to 5×10^{-10} mbar. Typical settings of transmission mode and SID experiments can be found in the Supporting Information (Table S1). Data were acquired at resolution settings corresponding to 2 s transients with transient averaging disabled. To lower the number of ions entering the Orbitrap analyzer, samples were diluted to concentrations between 50–500 nM, while sample concentrations for SID were in the 1–3 µM regime. In addition, automatic gain control (AGC) was disabled, and injection times were manually set between 0.03-1 ms to maximize individual ion acquisition by optimally populating available charge state and isotopic channels while minimizing multi-ions events which correspond to the collection of multiple ions at a singular frequency value. To achieve single ion measurement, the number of individual ion signals collected was decreased to ~100 per scan event. The charge calibration was generated by nano electrospray of various proteins with known charge states: streptavidin, C reactive protein, pyruvate kinase, glutamate dehydrogenase, and GroEL.

Data processing

All raw signal ion data were first filtered by STORIboard software (Thermo Fisher Scientific) using R Squared threshold 0.99, duration threshold 0.42 s,maximum time of birth 0.1 s, and signal to noise threshold 1. R Squared ensures a linear STORI slope and the duration threshold ensures the ion persists long enough to enable accurate charge assignment. The max time of birth ensures that the birth of that new frequency value is excluded from processing if any fragmentation occurs within the orbitrap. The STORI slopes for unknown species were converted to charges using a calibration generated from protein standards with known charge states, described in Figure S1. The charge vs. *m/z* and mass vs. *m/z* were plotted using a house-built Python-based data processing algorithm. The CDMS data were processed and deconvolved using UniDec CD.[51] Detailed data processing parameters are described in Supporting Information.

Results and Discussion

CDMS resolves the extensive SID fragments of GroEL. The SID-CDMS approach is firstly applied on a homomeric protein standard GroEL, a tetradecameric protein complex (801 kDa) consisting of two stacked heptamer rings.[53] Upon activation by SID, GroEL dissociates into a wide variety of products, ranging from monomers to tridecamers and including heptamers that reflect the stacked-heptamer structure.[54] Those extensive fragments are informative to characterize the structure, but they also add complexity to the spectra due to overlapping charge states of different oligomers, making the product assignment ambiguous, especially for the hexamers which can overlap with dimers and trimers. Previously, SID of GroEL was done on a quadrupole time-of-flight (Q-TOF) instrument and ion mobility was used to separate *m/z* overlapping fragments.[54] Although this identified different fragments of GroEL, it is still difficult to resolve all possible oligomers in the overlapping region because of the low *m/z* resolution and arrival time distribution broadening due to the partial restructuring of the ions. To overcome those challenges, SID on the Orbitrap platform was coupled with CDMS, which nicely resolved the overlapping *m/z* fragments.

GroEL tetradecamer in 200mM ammonium acetate solution results in a charge state distribution with the 66+ charge state as the dominant peak. The whole charge state distribution was selected and subjected to SID voltage 135 V, yielding a variety of fragments ranging from monomers to tetradecamers which is consistent with the observation of SID for GroEL in AmAc on the Q-TOF platform.[54] These extensive fragments, along with the charge-stripped tetradecamers are well resolved and separated by charge and *m/z*, as demonstrated in Figure 1A. The ambiguous product peaks at *m/z* 11440 Da in past SID experiments with TOF platforms have been resolved as hexamer 30+, pentamer 25+, tetramer 20+, trimer 15+, and dimer 10+ in CDMS (Figure 1C). The monomer 5+ at that m/z value is not detected due to the lowest charge detection limit of proteins (~5+ to 6+). In this instance, the direct measurement of the charge state allows for the direct observation of oligomeric states that overlap in *m/z*. The monomer and dimer product ions are dominant fragments, suggesting that the dissociation pathway follows the ejection of small subunits (monomers, dimers) from different allosteric states of GroEL. In the absence of ATP binding, the GroEL heptameric ring adopts the taut (T) state, which allows for additional salt bridge formation between the adjacent monomers, as indicated by the dimer formation of the allosteric probe.[55] The relaxed (R) state is dominant when bound to ATP, and the monomer ejection is predicted to be preferred because all monomers interact loosely in the R state.[56] The relatively high abundance of dimers and the complementary dodecamers indicates that they may be cleaved from the T-state rings. The presence of monomers suggests the secondary dissociation or direct fragmentation from the R state due to restructuring. The restructuring can be further suppressed with charge reduction in the solution phase (Figure S2). There are also heptamers present in higher abundance compared to the adjacent fragments (trimers, tetramers, pentamers, and hexamers) in the spectrum (Figure 1A and 1B). The heptamer peaks within the *m/z* range of 11000−16000

correspond to charge states from 36+ to 26+, which are around half the charge states of the tetradecamer precursor (69+~62+). This indicates that there is a portion of tetradecamer undergoing the dissociation pathway that produces heptamers in a symmetric manner, representative of its native quaternary structure (two stacked heptamer rings). (In previous work, we showed that charge reduction in solution generates GroEL 14-mers that produce higher abundance 7-mer than produced from "normal charge" GroEL).The dominant charge state of heptamer is 31+ , a value smaller than half of the dominant charge state of tetradecamer 66+. This pathway is possible from the dissociation of precursors with lower charge states, consistent with the previous observation that the precursors undergo charge stripping prior to dissociation.[57] The lower charge states help suppress the restructuring of the precursor and allow the native-like fragmentation pathway. The expected fragmentation pattern for GroEL shown in SID-CDMS demonstrates that this method enables the separation of the overlapping fragments from more complicated biological assembles, providing useful structural information even in the absence of ion mobility.

SID-CDMS reflects the structural topology of 20S proteasome. The human 20S proteasome is a hetero-oligomer (724 kDa, 28 subunits) composed of two outer heptameric rings containing α-type subunits, and two inner rings consisting of β-type subunits, stacked into a cylindrical structure ($\alpha_7\beta_7\beta_7\alpha_7$).[58] For human proteasomes, the α- and β- subunits of heptameric rings are closely related but non-identical, resulting in complexity in the tandem mass spectra. Multiple proteoforms have been observed for both α and β subunits, bringing an additional level of heterogeneity to characterization.[59, 60]

The whole charge state distribution of proteasome was isolated, dissociated using SID at 105 V, and then detected by CDMS (intensity-*m/z* and charge-*m/z* plots shown in Figure S3). The unresolved intensity-*m/z* spectrum was separated by adding charge detection and interpreted to mass outputs using the house-built Python algorithm. Multiple SID fragments were plotted in mass-*m/z* as shown in Figure 2A: free α containing subunits, α_7 rings, half proteasomes ($\alpha_7\beta_7$), $\beta_7\beta_7\alpha_7$ particles (20S-α_7), and subcomplexes of the proteasome that are missing one or two α subunits. The most abundant fragments are the free α_7 rings, revealing that the α-β interface is relatively weaker than the β-β interface. This is consistent with a previous PISA interfacial analysis that showed the α-β interface has a smaller interface area, fewer hydrogen bonds, and fewer salt bridges compared to the β-β interface.[58, 60] The half proteasomes ($\alpha_7\beta_7$) are also observed, suggesting that the dissociation energy is sufficient to cleave the β-β interface, either from the intact precursor or after loss of the α7 ring. 20S-α_7 are the complementary fragments of the α_7 ring and, without CDMS or IM, those peaks can be difficult to assign with confidence because their *m/z* range overlaps with the region of the charge-stripped precursor, half proteasomes, and 20S-α and 20S-2α. The charge measurement capability of CDMS allows for the direct observation of those SID products that overlap in *m/z* space. 20S-α and 20S-2α fragments have been respectively reported in SID results using ion mobility or Orbitrap without CDMS. Due to the heterogeneity of α subunits and salt adducts, broader peaks are usually observed for 20S-α and 20S-2α fragments. The two distributions of 20S-α and 20S-2α can be discriminated in CDMS but the accurate mass assignment is still tough due to their low intensity. In addition to the cylindrical structure of the full proteasome, further structural information can be revealed by α-containing subunits. The α monomer, dimer, trimer, and tetramer peaks clustered in the *m/z* region 3000 to 7000 are directly differentiated in CDMS (Figure 2B). All seven α monomers are observed and the proteoforms of α monomers are identified by the exact masses (Table S3). The observed masses are sligjltly higher than the therotical masses due to adducting of solvents/salts. The complete connectivity of the α_7 ring, as demonstrated in the inset of Figure 2B, can be mapped by the α dimers and trimers. All surface collision products of proteosomes separated and characterized by CDMS together provide multiple layers of structural information for the hetero protein complexes including overall structure, connectivity, and proteoforms.

SID-CDMS dissects AAV capsids into multimers of trimeric fragments.

Adeno-associated viral (AAV) vectors are currently used as gene therapy delivery systems for various diseases.[61-64] The AAV capsid packages a 4.7-kb single-stranded DNA (ssDNA) genome. AAV capsids (~3.7 mega Dalton) contain 60 subunits of 3 distinct viral proteins (VPs) with an approximate ratio of 1:1:10.[65] VP2 and VP3 are truncations of VP1; VP3 is the shortest among the VPs and is a truncation of VP2.[66] Only the overlapping region in VP3 is resolved in the atomic resolution structures of AAVs determined by cryo-electron microscopy and X-ray crystallography due to the low abundance of VP1/2 and the disordered nature of the extra sequence stretches in VP1/2.[67] In the resolved structures of capsids, VP monomers assemble into a T=1 icosahedral capsid shell with 2-, 3-, and 5-fold symmetry axes.[65] There is a depression at the 2-fold symmetry axes contributing to conformational changes in response to pH.[68] The trimers with a 3-fold axis of symmetry protrude from the capsid surface and are responsible for receptor binding and antibody recognition. Five VP monomers form a pentamer with a 5-fold axis of symmetry leaving a channel pore in the center to link the inside virus to the outside environment.[69]

Characterization of AAVs, including the stoichiometry of VPs, and the purity of genome-loaded AAV, is essential in AAV preparations, but unfortunately many AAV companies currently make their meaurements by AUC (analytical ultracentrifugation) with a relatively large sample requirement. With low sample consumption and high accuracy, CDMS can resolve intermediate mass species, making it a unique technique for the quantitation of capsid populations.[70] Previous studies have focused on using CDMS to measure the intact mass of AAVs to determine the levels of empty, partially filled and fully filled capsids. There are few structural studies of AAVs using mass spectrometry because AAVs are found to be stable enough to survive traditional gas-phase activation, with little to no fragmentation seen.[23, 24, 28] In this sense, SID, which provides a larger collision target and higher-energy deposition, is found to be able to dissociate the intact capsids efficiently. The SID fragments of AAVs can be well-resolved when SID is coupled with CDMS, providing unique insights into AAV capsid structure.The intact mass of empty AAV8 was measured first by CDMS (intensity-*m/z* and mass-*m/z* plots shown in Figure S4) and the major population was 3.72 MDa corresponding to an empty capsid. There is also a minor population (4.14 MDa) with a mass higher than empty AAV8 possibly due to the possible incomplete removal of the genome. Ions in the *m/z* range of 20000-25000 for empty AAV8 were isolated and subjected to SID, resulting in a series of different fragments, each aligning with a different oligomeric state of the viral protein. At low SID voltage (125 V), fragments associated with trimer, hexamer, 9mer, 15mer, 30mer, and 45mer were observed (Figure 3). All those fragments are composed of VP trimers, which is consistent with the native topology of AAV, in that 20 VP trimers assemble into a 60mer capsid. Based on these results, trimers are predicted to be the relatively stable building block (the inner interface of trimers is slightly stronger than the outer). The fragmentation pattern matched the calculated interface areas of the capsid remarkably well. When considering the top 3 interfaces of the crystal structure using the PISA algorithm, the total interface areas required to cleave the VP trimer to monomers are 14880 $Å^2$ (3x4960 $Å^2$) which is much higher than the total interface between two trimers (6271 $Å^2$; 2x2364 $Å^2$ + 1x1543 $Å^2$).[71] This shows the tendency to cleave along the 2/5 fold wall primarily when colliding with the surface, releasing 15mer and 45mer. Both 15mer and 45mer can further dissociate at the weaker interfaces, producing additional fragments. Increasing the SID voltage allows higher-intensity monomers, dimers, trimers, tetramers, pentamers, and hexamers to be observed in the low *m/z* region. Some percentage of those extensive fragments may be due to the secondary dissociation from SID fragments, e.g., monomers and dimers are possible from trimers. Similarly, 9mers are likely to be the complementary fragments of hexamers released from the 15mer, based on the fact that the relative intensity of 15mer decreases compared to that in low energy SID. Validation of the secondary dissociation requires the collection of SID energy-resolved mass spectra or tandem SID in future work. In addition to the verification of AAV topology, SID-CDMS also shows the possibility of the direct examination of VP

composition from intact AAVs. The fragments below 15mer contain predominantly VP3 with different combinations of VPs found in 24mer, 30mer, and 45mer (Table S4). This is consistent with the fact that the VPs are the most abundant viral proteins with a theoretical percentage of over 83%. The additional sequences in VP2 and VP3 might also provide extra interactions locally, making them harder to cleave.

Conclusion

SID produces structural details for protein complexes with informative fragments that are not observed in traditional activation methods. CDMS provides a straightforward solution to resolve extensive SID fragments on the Orbitrap platform by directly measuring the charge states of fragments that would otherwise overlap in nominal *m/z* space. In this work, we show the house-built Python algorithm for plotting the CDMS data (w/ SID) in charge-*m/z* or mass-*m/z* effectively extracts meaningful mass information directly from the otherwise unresolved and uninterpretable mass spectrum. More importantly, we demonstrate that SID coupled with CDMS is a powerful tool to study substructure and connectivity, especially for large and heterogeneous complexes. For GroEL, SID-CDMS reflects the stacked-ring structure, which is consistent with previous results on time-of-flight platforms coupled with ion mobility. In addition to the native structure of the 20S proteasome, multiple layers of structural information are provided in SID-CDMS, including subunit connectivity and proteoform information. For AAV capsids, SID-CDMS suggests that the 60mer capsid is assembled from 20 VP trimers as the monomer-monomer interface of the trimers has a higher interfacial strength than other interfaces in the capsid. The SID-CDMS integrated approach provides a means to better define the assembly of capsids and to engineer more stable vectors. SID-CDMS shows the potential to investigate the viral protein composition of intact capsids and will benefit from future improvements to the accuracy of charge assignment (e.g., longer transients in the Orbitrap).

Acknowledgements

The authors thank Mike Senko (Thermo Fisher Scientific) for his assistance with CDMS data processing using STORIboard and Neil Kelleher (Northwestern University) for initial collaboration of STORI method. The authors also thank Nicholas Horvath for his help in the testing of CDMS tuning and the collection of calibration curve. This work was funded by grants from National Institutes of Health [P41GM128577 to V.H.W.; P41GM108569 to N.L.K.].

Figures

Figure 0. Graphical abstract

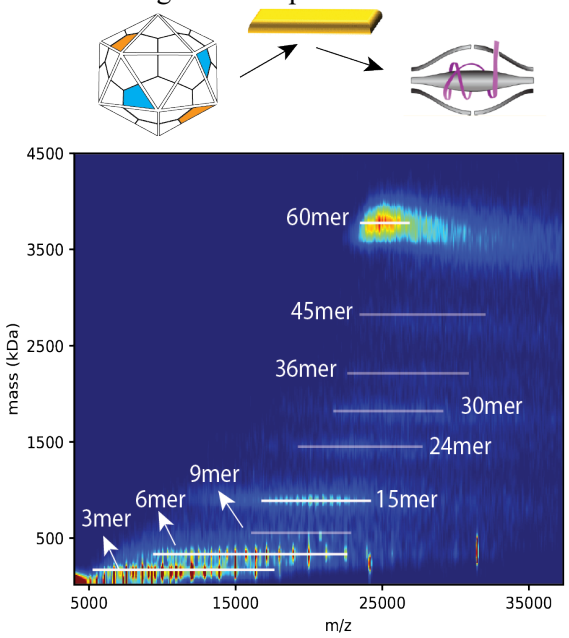

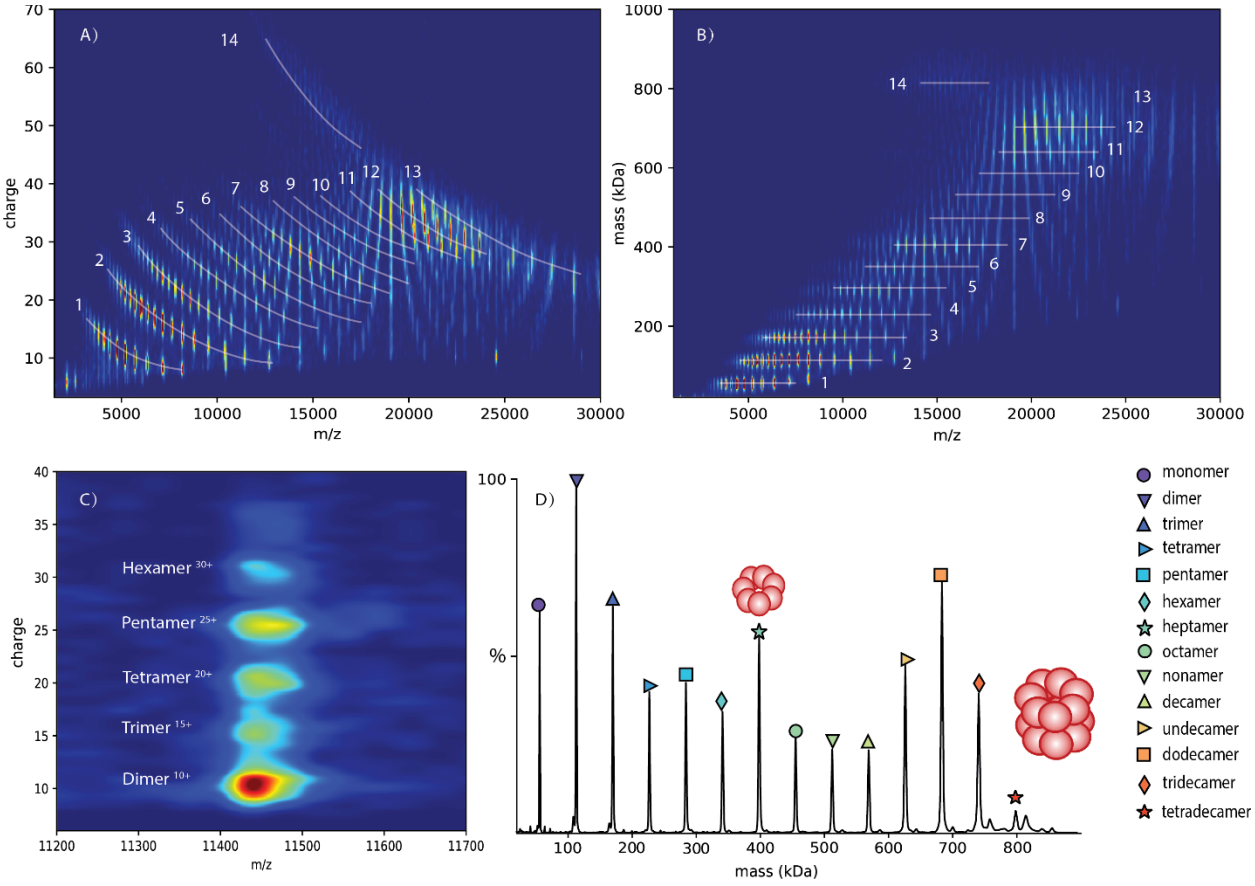

Figure 1. Charge-*m/z* plot (A) and mass−*m/z* plot (B) of the SID-CDMS spectra for GroEL tetradecamer at "normal" charge (as sprayed from ammonium acetate), acquired with an IST voltage of -50 V and an SID voltage of 135 V. The separation in charge states in the vertical axis assists in the discrimination of species that are overlapping in *m/z*. The charge distributions of ions are labeled at their approximate location with transparent white lines. The oligomeric states of GroEL from monomer to tetradecamer are indicated by a number from 1 to 15. (C) Zoomed-in view of charge-*m/z* plot at 11220-11700 Da. The *m/z* overlapping heptamer, hexamer, pentamer, tetramer, and trimer are well-resolved by charge states. (D) SID-CDMS spectrum was processed and deconvolved by UniDec CD to better view the relative intensity of SID products. The red inset structure is a cartoon representation of the GroEL tetradecamer.

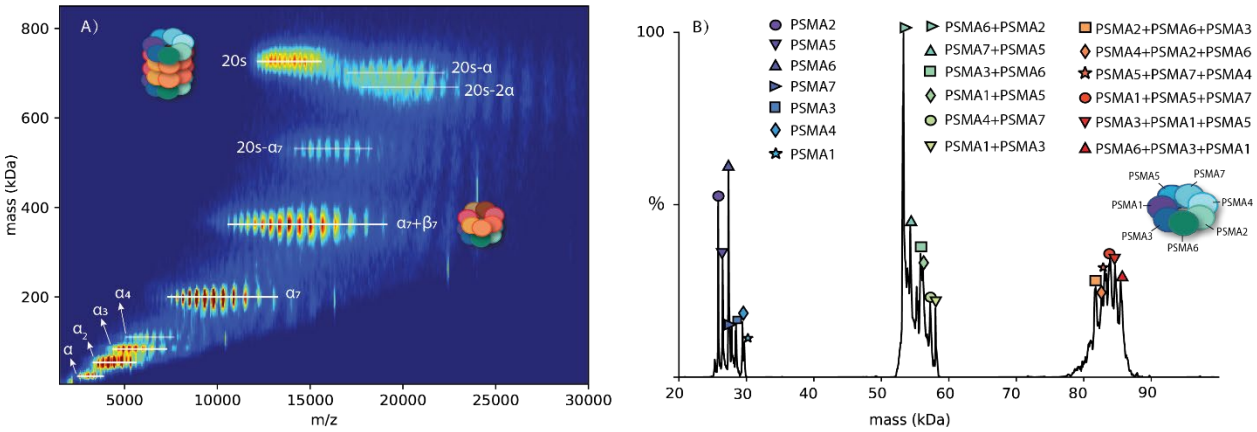

Figure 2. (A) Mass−*m/z* plot of the SID-CDMS spectra for human 20S proteasome, acquired with SID voltage of 105V. The charge distribution of ions is designated at their approximate location with white lines. The structure of the precursor and major dissociation products, α_7 and $\alpha_7\beta_7$ is graphically depicted in cartoon representation. (B) Zoomed-in view of the low mass region of the SID-CDMS spectrum processed and deconvolved by UniDec CD, highlighting α-monomers/dimers/ trimers. The inset cartoon representation shows the connectivity of the α_7 ring determined by the crystal structure.

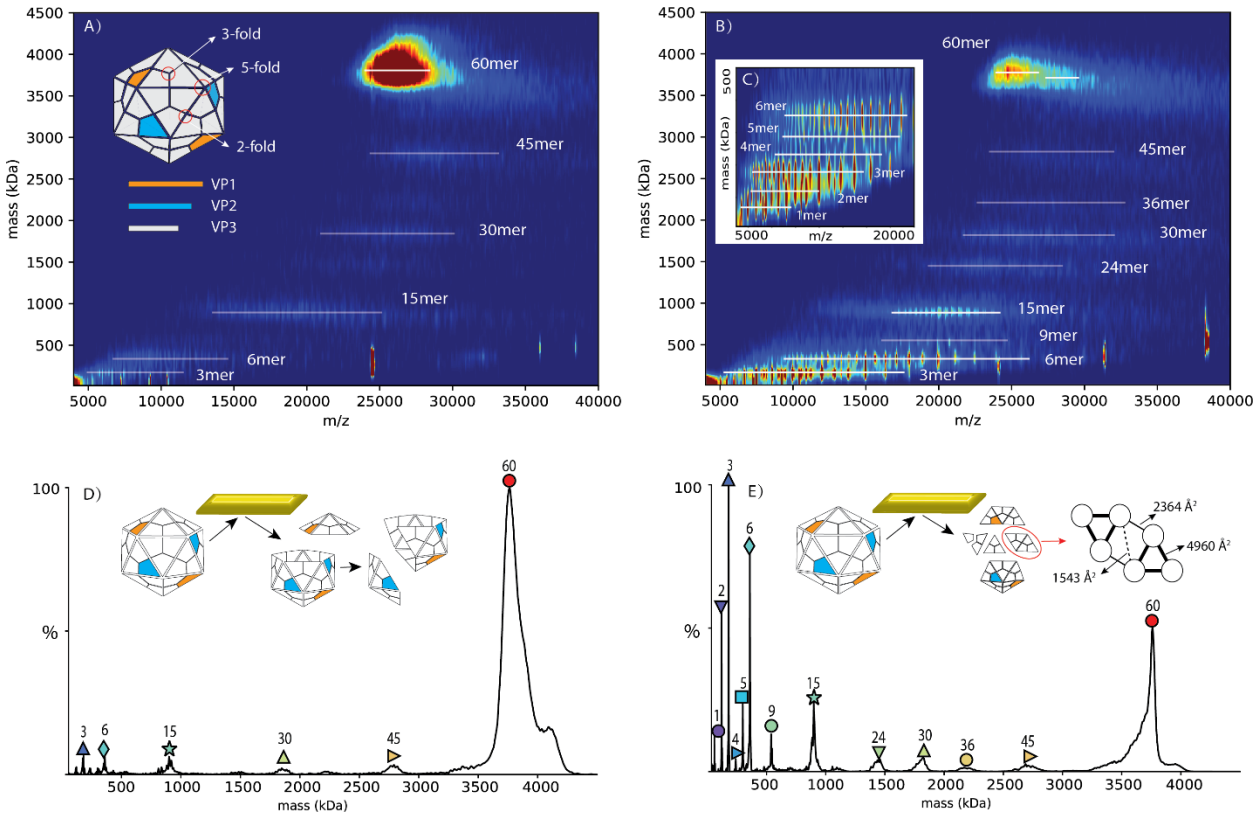

Figure 3. Low- and high-energy SID-CDMS of empty AAV8 capsids. (A) Mass−*m/z* plot of the SID spectra for AAV, acquired with a SID voltage of 125 V. Inset is a cartoon representation of the empty AAV8 capsid composed of sixty copied of viral proteins: VP1 (yellow), VP2 (blue), and VP3 (white). The approximate icosahedral 2-, 3-, and 5-fold axes are labeled. (B) Mass−*m/z* plot of the SID spectra for AAV, acquired with a SID voltage of 225 V. (C) Inset is the zoom-in of the low mass region, showing the smaller oligomeric fragments: from monomers to hexamers. (D) Deconvolved SID-CDMS at SID 225 V by UniDec CD. Numbers indicate the oligomer states. Inset is a cartoon representation showing the representative fragmentation pathway at low SID energy. The 60mer capsid dissociates along 2/5-fold axes into 15mer and 45mer; 45mer continues to dissociate into 15mer and 30mer. (E) Deconvolved SID-CDMS at SID 225 V by UniDec CD. Numbers indicate the oligomer states. Inset is a cartoon representation showing the representative fragmentation pathway at high SID energy. Small VP subunits (1mer, 2mer, 3mer, 6mer, 9mer, and 15mer) is observed. The interface areas of two trimers are determined by PISA analysis (PDB ID: 2QA0).

References

1. Heck, A. J. R., Native mass spectrometry: a bridge between interactomics and structural biology. *Nature Methods* **2008,** *5* (11), 927-933.
2. Lössl, P.; van de Waterbeemd, M.; Heck, A. J. R., The diverse and expanding role of mass spectrometry in structural and molecular biology. *The EMBO Journal* **2016,** *35* (24), 2634-2657.
3. Liko, I.; Allison, T. M.; Hopper, J. T. S.; Robinson, C. V., Mass spectrometry guided structural biology. *Current Opinion in Structural Biology* **2016,** *40*, 136-144.
4. Barth, M.; Schmidt, C., Native mass spectrometry—A valuable tool in structural biology. *Journal of Mass Spectrometry* **2020,** *55* (10), e4578.
5. Hernández, H.; Robinson, C. V., Determining the stoichiometry and interactions of macromolecular assemblies from mass spectrometry. *Nature Protocols* **2007,** *2* (3), 715-726.
6. Leney, A. C.; Heck, A. J. R., Native Mass Spectrometry: What is in the Name? *Journal of the American Society for Mass Spectrometry* **2017,** *28* (1), 5-13.
7. Mann, M.; Meng, C. K.; Fenn, J. B., Interpreting mass spectra of multiply charged ions. *Analytical Chemistry* **1989,** *61* (15), 1702-1708.
8. Rolland, A. D.; Prell, J. S., Approaches to Heterogeneity in Native Mass Spectrometry. *Chemical Reviews* **2022,** *122* (8), 7909-7951.
9. Keifer, D. Z.; Pierson, E. E.; Jarrold, M. F., Charge detection mass spectrometry: weighing heavier things. *Analyst* **2017,** *142* (10), 1654-1671.
10. Jarrold, M. F., Applications of Charge Detection Mass Spectrometry in Molecular Biology and Biotechnology. *Chemical Reviews* **2022,** *122* (8), 7415-7441.
11. Keifer, D. Z.; Shinholt, D. L.; Jarrold, M. F., Charge Detection Mass Spectrometry with Almost Perfect Charge Accuracy. *Analytical Chemistry* **2015,** *87* (20), 10330-10337.
12. Todd, A. R.; Barnes, L. F.; Young, K.; Zlotnick, A.; Jarrold, M. F., Higher Resolution Charge Detection Mass Spectrometry. *Analytical Chemistry* **2020,** *92* (16), 11357-11364.
13. Hogan, J. A.; Jarrold, M. F., Optimized Electrostatic Linear Ion Trap for Charge Detection Mass Spectrometry. *Journal of the American Society for Mass Spectrometry* **2018,** *29* (10), 2086-2095.
14. Elliott, A. G.; Harper, C. C.; Lin, H.-W.; Williams, E. R., Mass, mobility and MSn measurements of single ions using charge detection mass spectrometry. *Analyst* **2017,** *142* (15), 2760-2769.
15. Benner, W. H., A Gated Electrostatic Ion Trap To Repetitiously Measure the Charge and m/z of Large Electrospray Ions. *Analytical Chemistry* **1997,** *69* (20), 4162-4168.
16. Wörner, T. P.; Snijder, J.; Bennett, A.; Agbandje-McKenna, M.; Makarov, A. A.; Heck, A. J. R., Resolving heterogeneous macromolecular assemblies by Orbitrap-based single-particle charge detection mass spectrometry. *Nature Methods* **2020,** *17* (4), 395-398.
17. Kafader, J. O.; Melani, R. D.; Senko, M. W.; Makarov, A. A.; Kelleher, N. L.; Compton, P. D., Measurement of Individual Ions Sharply Increases the Resolution of Orbitrap Mass Spectra of Proteins. *Analytical Chemistry* **2019,** *91* (4), 2776-2783.
18. Kafader, J. O.; Melani, R. D.; Durbin, K. R.; Ikwuagwu, B.; Early, B. P.; Fellers, R. T.; Beu, S. C.; Zabrouskov, V.; Makarov, A. A.; Maze, J. T.; Shinholt, D. L.; Yip, P. F.; Tullman-Ercek, D.; Senko, M. W.; Compton, P. D.; Kelleher, N. L., Multiplexed mass spectrometry of individual ions improves measurement of proteoforms and their complexes. *Nature Methods* **2020,** *17* (4), 391-394.
19. McGee, J. P.; Melani, R. D.; Yip, P. F.; Senko, M. W.; Compton, P. D.; Kafader, J. O.; Kelleher, N. L., Isotopic Resolution of Protein Complexes up to 466 kDa Using Individual Ion Mass Spectrometry. *Analytical Chemistry* **2021,** *93* (5), 2723-2727.
20. Lai, S.-H.; Tamara, S.; Heck, A. J. R., Single-particle mass analysis of intact ribosomes by mass photometry and Orbitrap-based charge detection mass spectrometry. *iScience* **2021,** *24* (11), 103211.
21. Miller, L. M.; Bond, K. M.; Draper, B. E.; Jarrold, M. F., Characterization of Classical Vaccines by Charge Detection Mass Spectrometry. *Analytical Chemistry* **2021,** *93* (35), 11965-11972.

22. Pierson, E. E.; Keifer, D. Z.; Kukreja, A. A.; Wang, J. C. Y.; Zlotnick, A.; Jarrold, M. F., Charge Detection Mass Spectrometry Identifies Preferred Non-Icosahedral Polymorphs in the Self-Assembly of Woodchuck Hepatitis Virus Capsids. *Journal of Molecular Biology* **2016,** *428* (2, Part A), 292-300.
23. Pierson, E. E.; Keifer, D. Z.; Asokan, A.; Jarrold, M. F., Resolving Adeno-Associated Viral Particle Diversity With Charge Detection Mass Spectrometry. *Analytical Chemistry* **2016,** *88* (13), 6718-6725.
24. Wörner, T. P.; Bennett, A.; Habka, S.; Snijder, J.; Friese, O.; Powers, T.; Agbandje-McKenna, M.; Heck, A. J. R., Adeno-associated virus capsid assembly is divergent and stochastic. *Nature Communications* **2021,** *12* (1), 1642.
25. Kostelic, M. M.; Ryan, J. P.; Brown, L. S.; Jackson, T. W.; Hsieh, C.-C.; Zak, C. K.; Sanders, H. M.; Liu, Y.; Chen, V. S.; Byrne, M.; Aspinwall, C. A.; Baker, E. S.; Marty, M. T., Stability and Dissociation of Adeno-Associated Viral Capsids by Variable Temperature-Charge Detection-Mass Spectrometry. *Analytical Chemistry* **2022,** *94* (34), 11723-11727.
26. Barnes, L. F.; Draper, B. E.; Jarrold, M. F., Analysis of thermally driven structural changes, genome release, disassembly, and aggregation of recombinant AAV by CDMS. *Molecular Therapy - Methods & Clinical Development* **2022,** *27*, 327-336.
27. Barnes, L. F.; Draper, B. E.; Kurian, J.; Chen, Y.-T.; Shapkina, T.; Powers, T. W.; Jarrold, M. F., Analysis of AAV-Extracted DNA by Charge Detection Mass Spectrometry Reveals Genome Truncations. *Analytical Chemistry* **2023,** *95* (9), 4310-4316.
28. Barnes, L. F.; Draper, B. E.; Chen, Y.-T.; Powers, T. W.; Jarrold, M. F., Quantitative analysis of genome packaging in recombinant AAV vectors by charge detection mass spectrometry. *Molecular Therapy - Methods & Clinical Development* **2021,** *23*, 87-97.
29. Wörner, T. P.; Snijder, J.; Friese, O.; Powers, T.; Heck, A. J. R., Assessment of genome packaging in AAVs using Orbitrap-based charge-detection mass spectrometry. *Molecular Therapy - Methods & Clinical Development* **2022,** *24*, 40-47.
30. Benesch, J. L. P.; Aquilina, J. A.; Ruotolo, B. T.; Sobott, F.; Robinson, C. V., Tandem Mass Spectrometry Reveals the Quaternary Organization of Macromolecular Assemblies. *Chemistry & Biology* **2006,** *13* (6), 597-605.
31. Sharon, M., How far can we go with structural mass spectrometry of protein complexes? *Journal of the American Society for Mass Spectrometry* **2010,** *21* (4), 487-500.
32. Skinner, O. S.; Haverland, N. A.; Fornelli, L.; Melani, R. D.; Do Vale, L. H. F.; Seckler, H. S.; Doubleday, P. F.; Schachner, L. F.; Srzentić, K.; Kelleher, N. L.; Compton, P. D., Top-down characterization of endogenous protein complexes with native proteomics. *Nature Chemical Biology* **2018,** *14* (1), 36-41.
33. Karch, K. R.; Snyder, D. T.; Harvey, S. R.; Wysocki, V. H., Native Mass Spectrometry: Recent Progress and Remaining Challenges. *Annual Review of Biophysics* **2022**.
34. Sciuto, S. V.; Liu, J.; Konermann, L., An Electrostatic Charge Partitioning Model for the Dissociation of Protein Complexes in the Gas Phase. *Journal of the American Society for Mass Spectrometry* **2011,** *22* (10).
35. Popa, V.; Trecroce, D. A.; McAllister, R. G.; Konermann, L., Collision-Induced Dissociation of Electrosprayed Protein Complexes: An All-Atom Molecular Dynamics Model with Mobile Protons. *The Journal of Physical Chemistry B* **2016,** *120* (23), 5114-5124.
36. Sinelnikov, I.; Kitova, E. N.; Klassen, J. S., Influence of coulombic repulsion on the dissociation pathways and energetics of multiprotein complexes in the gas phase. *Journal of the American Society for Mass Spectrometry* **2007,** *18* (4), 617-631.
37. Stiving, A. Q.; VanAernum, Z. L.; Busch, F.; Harvey, S. R.; Sarni, S. H.; Wysocki, V. H., Surface-Induced Dissociation: An Effective Method for Characterization of Protein Quaternary Structure. *Analytical Chemistry* **2019,** *91* (1), 190-209.
38. Harvey, S. R.; Ben-Nissan, G.; Sharon, M.; Wysocki, V. H., Surface-Induced Dissociation for Protein ComplexProtein complexes Characterization. In *Proteoform Identification: Methods and Protocols*, Sun, L.; Liu, X., Eds. Springer US: New York, NY, 2022; pp 211-237.

39. VanAernum, Z. L.; Gilbert, J. D.; Belov, M. E.; Makarov, A. A.; Horning, S. R.; Wysocki, V. H., Surface-Induced Dissociation of Noncovalent Protein Complexes in an Extended Mass Range Orbitrap Mass Spectrometer. *Analytical Chemistry* **2019,** *91* (5), 3611-3618.
40. Zhou, M.; Huang, C.; Wysocki, V. H., Surface-Induced Dissociation of Ion Mobility-Separated Noncovalent Complexes in a Quadrupole/Time-of-Flight Mass Spectrometer. *Analytical Chemistry* **2012,** *84* (14), 6016-6023.
41. Snyder, D. T.; Panczyk, E. M.; Somogyi, A.; Kaplan, D. A.; Wysocki, V., Simple and Minimally Invasive SID Devices for Native Mass Spectrometry. *Analytical Chemistry* **2020,** *92* (16), 11195-11203.
42. Zhou, M.; Dagan, S.; Wysocki, V. H., Impact of charge state on gas-phase behaviors of noncovalent protein complexes in collision induced dissociation and surface induced dissociation. *Analyst* **2013,** *138* (5), 1353-1362.
43. Zhou, M.; Wysocki, V. H., Surface Induced Dissociation: Dissecting Noncovalent Protein Complexes in the Gas phase. *Accounts of Chemical Research* **2014,** *47* (4), 1010-1018.
44. Song, Y.; Nelp, M. T.; Bandarian, V.; Wysocki, V. H., Refining the Structural Model of a Heterohexameric Protein Complex: Surface Induced Dissociation and Ion Mobility Provide Key Connectivity and Topology Information. *ACS Central Science* **2015,** *1* (9), 477-487.
45. Quintyn, R. S.; Zhou, M.; Yan, J.; Wysocki, V. H., Surface-Induced Dissociation Mass Spectra as a Tool for Distinguishing Different Structural Forms of Gas-Phase Multimeric Protein Complexes. *Analytical Chemistry* **2015,** *87* (23), 11879-11886.
46. Harvey, S. R.; Seffernick, J. T.; Quintyn, R. S.; Song, Y.; Ju, Y.; Yan, J.; Sahasrabuddhe, A. N.; Norris, A.; Zhou, M.; Behrman, E. J.; Lindert, S.; Wysocki, V. H., Relative interfacial cleavage energetics of protein complexes revealed by surface collisions. *Proceedings of the National Academy of Sciences* **2019,** *116* (17), 8143-8148.
47. Kafader, J. O.; Beu, S. C.; Early, B. P.; Melani, R. D.; Durbin, K. R.; Zabrouskov, V.; Makarov, A. A.; Maze, J. T.; Shinholt, D. L.; Yip, P. F.; Kelleher, N. L.; Compton, P. D.; Senko, M. W., STORI Plots Enable Accurate Tracking of Individual Ion Signals. *Journal of the American Society for Mass Spectrometry* **2019,** *30* (11), 2200-2203.
48. Wang, D.; Tai, P. W. L.; Gao, G., Adeno-associated virus vector as a platform for gene therapy delivery. *Nature Reviews Drug Discovery* **2019,** *18* (5), 358-378.
49. Wright, J. F. J. B. J., Quality control testing, characterization and critical quality attributes of adeno-associated virus vectors used for human gene therapy. **2021,** *16* (1), 2000022.
50. Li, C.; Samulski, R. J. J. N. R. G., Engineering adeno-associated virus vectors for gene therapy. **2020,** *21* (4), 255-272.
51. Kostelic, M. M.; Zak, C. K.; Liu, Y.; Chen, V. S.; Wu, Z.; Sivinski, J.; Chapman, E.; Marty, M. T., UniDecCD: Deconvolution of Charge Detection-Mass Spectrometry Data. *Analytical Chemistry* **2021,** *93* (44), 14722-14729.
52. Voziyan, P. A.; Fisher, M. T., Chaperonin-assisted folding of glutamine synthetase under nonpermissive conditions: Off-pathway aggregation propensity does not determine the co-chaperonin requirement. *Protein Science* **2000,** *9* (12), 2405-2412.
53. Braig, K.; Otwinowski, Z.; Hegde, R.; Boisvert, D. C.; Joachimiak, A.; Horwich, A. L.; Sigler, P. B., The crystal structure of the bacterial chaperonln GroEL at 2.8 Å. *Nature* **1994,** *371* (6498), 578-586.
54. Zhou, M.; Jones, C. M.; Wysocki, V. H., Dissecting the Large Noncovalent Protein Complex GroEL with Surface-Induced Dissociation and Ion Mobility–Mass Spectrometry. *Analytical Chemistry* **2013,** *85* (17), 8262-8267.
55. Corsepius, N. C.; Lorimer, G. H., Measuring how much work the chaperone GroEL can do. *Proceedings of the National Academy of Sciences* **2013,** *110* (27), E2451-E2459.
56. Hyeon, C.; Lorimer, G. H.; Thirumalai, D., Dynamics of allosteric transitions in GroEL. *Proceedings of the National Academy of Sciences* **2006,** *103* (50), 18939-18944.
57. Snyder, D. T.; Harvey, S. R.; Wysocki, V. H., Surface-induced Dissociation Mass Spectrometry as a Structural Biology Tool. *Chemical Reviews* **2021**.

58. Schrader, J.; Henneberg, F.; Mata, R. A.; Tittmann, K.; Schneider, T. R.; Stark, H.; Bourenkov, G.; Chari, A., The inhibition mechanism of human 20S proteasomes enables next-generation inhibitor design. *Science* **2016,** *353* (6299), 594-598.
59. Harvey, S. R.; VanAernum, Z. L.; Wysocki, V. H., Surface-Induced Dissociation of Anionic vs Cationic Native-Like Protein Complexes. *Journal of the American Chemical Society* **2021,** *143* (20), 7698-7706.
60. Vimer, S.; Ben-Nissan, G.; Morgenstern, D.; Kumar-Deshmukh, F.; Polkinghorn, C.; Quintyn, R. S.; Vasil'ev, Y. V.; Beckman, J. S.; Elad, N.; Wysocki, V. H.; Sharon, M., Comparative Structural Analysis of 20S Proteasome Ortholog Protein Complexes by Native Mass Spectrometry. *ACS Central Science* **2020,** *6* (4), 573-588.
61. Mingozzi, F.; High, K. A. J. N. r. g., Therapeutic in vivo gene transfer for genetic disease using AAV: progress and challenges. **2011,** *12* (5), 341-355.
62. Phase, I.; IIPhase II, I. P. J. n. r.; DIScoVery, D., The clinical landscape for AAV gene therapies. **2021,** *20*, 173.
63. Weinberg, M. S.; Samulski, R. J.; McCown, T. J. J. N., Adeno-associated virus (AAV) gene therapy for neurological disease. **2013,** *69*, 82-88.
64. Flotte, T. R.; Cataltepe, O.; Puri, A.; Batista, A. R.; Moser, R.; McKenna-Yasek, D.; Douthwright, C.; Gernoux, G.; Blackwood, M.; Mueller, C. J. N. m., AAV gene therapy for Tay-Sachs disease. **2022,** *28* (2), 251-259.
65. Drouin, L. M.; Agbandje-McKenna, M., Adeno-associated virus structural biology as a tool in vector development. *Future Virology* **2013,** *8* (12), 1183-1199.
66. Naumer, M.; Sonntag, F.; Schmidt, K.; Nieto, K.; Panke, C.; Davey Norman, E.; Popa-Wagner, R.; Kleinschmidt Jürgen, A., Properties of the Adeno-Associated Virus Assembly-Activating Protein. *Journal of Virology* **2012,** *86* (23), 13038-13048.
67. Mietzsch, M.; Pénzes, J. J.; Agbandje-McKenna, M. Twenty-Five Years of Structural Parvovirology *Viruses* [Online], 2019.
68. Nam, H.-J.; Gurda Brittney, L.; McKenna, R.; Potter, M.; Byrne, B.; Salganik, M.; Muzyczka, N.; Agbandje-McKenna, M., Structural Studies of Adeno-Associated Virus Serotype 8 Capsid Transitions Associated with Endosomal Trafficking. *Journal of Virology* **2011,** *85* (22), 11791-11799.
69. Tseng, Y.-S.; Gurda Brittney, L.; Chipman, P.; McKenna, R.; Afione, S.; Chiorini John, A.; Muzyczka, N.; Olson Norman, H.; Baker Timothy, S.; Kleinschmidt, J.; Agbandje-McKenna, M., Adeno-Associated Virus Serotype 1 (AAV1)- and AAV5-Antibody Complex Structures Reveal Evolutionary Commonalities in Parvovirus Antigenic Reactivity. *Journal of Virology* **2015,** *89* (3), 1794-1808.
70. Werle, A. K.; Powers, T. W.; Zobel, J. F.; Wappelhorst, C. N.; Jarrold, M. F.; Lyktey, N. A.; Sloan, C. D. K.; Wolf, A. J.; Adams-Hall, S.; Baldus, P.; Runnels, H. A., Comparison of analytical techniques to quantitate the capsid content of adeno-associated viral vectors. *Molecular Therapy - Methods & Clinical Development* **2021,** *23*, 254-262.
71. Nam, H.-J.; Lane Michael, D.; Padron, E.; Gurda, B.; McKenna, R.; Kohlbrenner, E.; Aslanidi, G.; Byrne, B.; Muzyczka, N.; Zolotukhin, S.; Agbandje-McKenna, M., Structure of Adeno-Associated Virus Serotype 8, a Gene Therapy Vector. *Journal of Virology* **2007,** *81* (22), 12260-12271.